AGU PUBLICATIONS

JGR

Journal of Geophysical Research: Space Physics

RESEARCH ARTICLE
10.1002/2014JA020621

Key Points:
- Intraplate strike slip earthquakes can Induce TEC anomalies in the ionosphere
- TEC perturbation split into two different modes propagating with different speeds north and south of the epicenter
- Anistropy of Rayleigh wave radiation pattern is the most feasible candidate for the observed N-S CID asymmetry

Supporting Information:
- Text S1 and Figures S1–S4
- Figure S1
- Figure S2
- Figure S3
- Figure S4

Correspondence to:
J. K. Catherine,
joshicatherine@yahoo.co.in

Citation:
Catherine, J. K., M. S. M. Vijayan, U. B. Syeda Rabiya, K. Shimna, V. K. Gahalaut, and D. S. Ramesh (2015), Dichotomy in mode propagation of coseismic ionospheric disturbance: Observations from 11 April 2012 Indian Ocean earthquake, *J. Geophys. Res. Space Physics*, *120*, doi:10.1002/2014JA020621.

Received 16 SEP 2014
Accepted 2 APR 2015
Accepted article online 13 APR 2015

©2015. American Geophysical Union. All Rights Reserved.

Dichotomy in mode propagation of coseismic ionospheric disturbance: Observations from 11 April 2012 Indian Ocean earthquake

J. K. Catherine[1], M. S. M. Vijayan[2], U. B. Syeda Rabiya[1], K. Shimna[2], Vineet K. Gahalaut[1], and D. S. Ramesh[3]

[1]CSIR-National Geophysical Research Institute, Hyderabad, India, [2]CSIR Fourth Paradigm Institute, Bangalore, India, [3]Indian Institute of Geomagnetism, Mumbai, India

Abstract The ionosphere response to the great intraplate Indian Ocean earthquake of 11 April 2012 (M_w 8.6) and its largest aftershock (M_w 8.2) is analyzed using GPS-aided total electron content (TEC) measurements. Data from the dense GPS networks, SuGAr (Sumatran GPS Array) and the permanent Andaman-Nicobar array, formed the near-field observations at distances 250–1200 km from the epicenter. Stations such as IISC, DGAR, and few others provided measurements over 2000 km from the epicenter. The coseismic ionospheric disturbances (CIDs) with a propagation velocity of 930–1262 m/s, equals the speeds of the shock acoustic waves, arrive within 10–18 min after the earthquake occurrence. The observed phenomenon of CID splitting into two modes, north and south of the epicenter, is akin to the well-documented effects of anisotropy on wave propagation. Closer to the epicenter, to its south, the propagation velocity of CID is ~1 km/s, and farther southeast of the network the velocity reduces to 500–600 m/s. In contrast, toward Andaman in the north, the CID propagation velocity increases to 2–3.5 km/s. The zenith angle of the line of sight between the GPS receiver and satellite appears to influence the amplitude of the TEC fluctuations. The anomalous azimuthal variation of the Rayleigh wave radiation pattern best explains the observed N-S asymmetry of CID.

1. Introduction

It is well established that strong earthquakes stimulate ionospheric perturbation due to earth-atmosphere coupling [*Artru et al*., 2004; *Lognonné et al*., 1998]. Operation of dense regional and international GPS networks in a continuous mode with high accuracy of phase measurements made it possible to investigate ionospheric disturbances caused by earthquakes at locations not only close to the epicenter but even at farther distances. Numerous studies have been carried out to understand the ionospheric disturbances induced by strong earthquakes [*Afraimovich et al*., 2001; *Calais and Minster*, 1995, 1998; *Ducic et al*., 2003; *Heki and Ping*, 2005; *Liu et al*., 2010, 2011]. Atmospheric waves caused by an earthquake that propagate in the vertical and/or radial directions interact with the ionosphere and perturb the total electron content (TEC), which is measured along the line of sight between the satellite and observation point with a GPS receiver. These disturbances are termed as coseismic ionospheric disturbances (CIDs). Their propagation velocities can match with that of Rayleigh, acoustic and gravity waves [*Afraimovich et al*., 2001; *Artru et al*., 2004; *Astafyeva et al*., 2009; *Calais and Minster*, 1995; *Davies*, 1990; *Ducic et al*., 2003; *Liu et al*., 2006; *Rolland et al*., 2011; *Yuen et al*., 1969].

It is generally perceived that dip-slip earthquakes of magnitude $M > 7$ occurring in subduction zones are expected to induce TEC fluctuations [*Calais and Minster*, 1995; *Heki and Ping*, 2005; *Rolland et al*., 2013]. However, TEC observations related to earthquakes with strike-slip mechanisms are rather sparse [*Astafyeva et al*., 2014]. In this context, with significant improvement in station density and processing tools together with recorded occurrence of great earthquakes in other tectonic environments, observations related to earthquakes other than subduction zone dip-slip events are accruing. The greatest instrumentally recorded intraplate strike-slip earthquake of magnitude (M_w) 8.6 occurred in the Indian Ocean off the west coast of northern Sumatra on 11 April 2012 at 08:38:37 UTC and is located about 100 km southwest of Sumatra trench. A great aftershock of magnitude (M_w) 8.2 with a strike-slip source mechanism followed 2 h later (at 10:43:09 UTC) at about 180 km south of the main shock (Figure 1a). The finite-fault slip model for the main shock presented by *Yue et al*. [2012] shows a maximum vertical displacement of 1–1.5 m at the

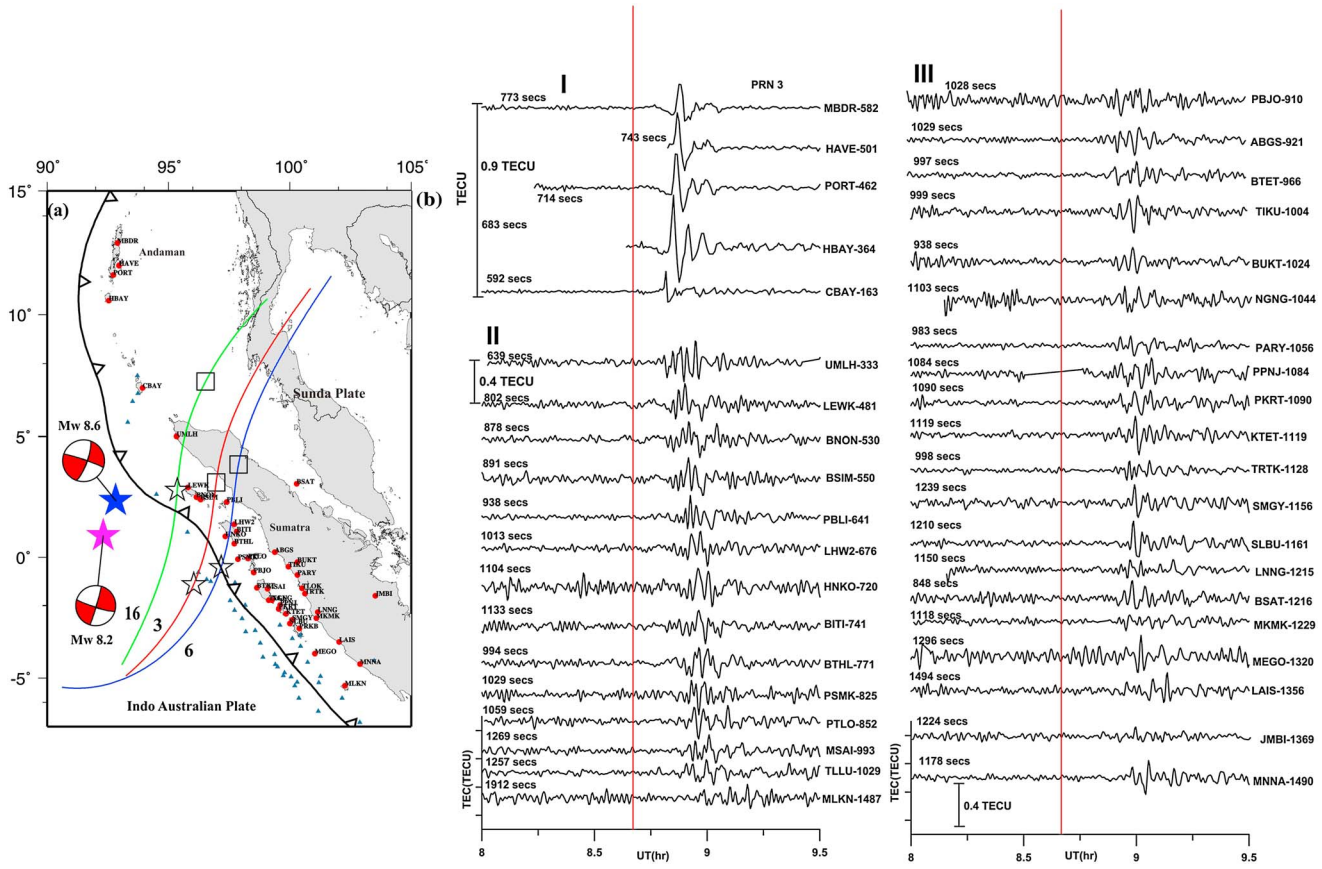

Figure 1. (a) Locations of GPS stations of Sumatra and Andaman used in the present study. GPS sites are marked by the red solid circles, and the SIPs of satellite 3 are marked by blue triangles. The colored stars show the epicenters of the main shock (M_w 8.6) and aftershock (M_w 8.2), respectively. Red, blue, and green solid curves represent the trajectories of satellites 3, 6, and 16, respectively. Black open stars along the trajectories are the SIPs of the CID arrival for the main shock at site LEWK. Black open squares along the trajectories are SIPs at the time of aftershock at 10:43 (UTC). Beach balls indicate the focal mechanism of two earthquakes. (b) Traces of band pass-filtered (1–10 min) coseismic TEC variation as observed by GPS satellite PRN 3. The vertical line indicates the origin time of the main shock. Distances of the SIPs of GPS sites from the epicenter are indicated on the right side and on the left side is the CID arrival time at that particular site after the earthquake.

source (Figure 3a). GPS sites in the southeast quadrant of the Sumatra region recorded horizontal coseismic displacements (~10–30 mm) in the northwest direction, while sites in the northwest Sumatra region experienced coseismic horizontal displacements (300–100 mm) in the northeast direction. These sites located at distances, both, close to the epicenter and farther, cover an observation range of 350 to 750 km. In contrast, GPS sites in the Andaman-Nicobar Islands at a distance of 500–1200 km north of the earthquake epicenter recorded ~40–15 mm southward coseismic horizontal displacements [*Yadav et al.*, 2013]. Aside from the above listed unique attributes of this great earthquake, the manifested relatively smaller vertical displacements both at the source and away, complex rupture of the earthquake [*Meng et al.*, 2012], and the powerful surface waves it generated [*Pollitz et al.*, 2012] prompted us to investigate whether such large seismic events in an intraplate environment can also perturb the TEC of ionosphere.

With this background, in the present study, the ionospheric response of the 11 April 2012 great Indian Ocean earthquake is documented using GPS measurements from locations close to the epicenter and far from it. Our results clearly demonstrate that the greatest intraplate strike-slip earthquake of the Indian Ocean which caused a maximum vertical displacement on the order of ~1.5 m could also trigger TEC fluctuations in the ionosphere both in the near field (Sumatra-Andaman) and far field (at Global Navigation Satellite Systems GPS sites which are at a distance of >2000 km). The phenomenon of CID extricating into fast and slow modes of propagation is pragmatic in the present study.

2. Methods of GPS Data Processing

Dual-frequency measurements (1.2 and 1.5 GHz) from GPS satellites located ~20,000 km above the Earth's surface provide integral information of the ionosphere by computing the differential code and carrier phase measurements recorded by ground-based GPS receivers. TEC calculation methods are described in detail in a number of earlier publications [e.g., *Afraimovich et al*., 2001; *Calais and Minster*, 1995; *Carrano and Groves*, 2009].

The integrated electron content (IEC) along the satellite-receiver path is then estimated using phase (IEC_φ) and code (IEC_p) measurements

$$IEC_\varphi = \frac{1}{40.3}\left[\frac{f_1^2 f_2^2}{f_1^2 - f_2^2}\right](L_1\lambda_1 - L_2\lambda_2) + B \tag{1}$$

$$IEC_p = \frac{1}{40.3}\left[\frac{f_1^2 f_2^2}{f_1^2 - f_2^2}\right](P_2 - P_1) + B \tag{2}$$

where L_1 and L_2 represent the carrier phase measurements; P_1 and P_2 are code measurements of frequencies f_1 and f_2, respectively; λ_1 and λ_2 stand for the corresponding wavelengths; $L_1\,\lambda_1$ and $L_2\,\lambda_2$ are additional paths of radio signal caused by the phase delay in the ionosphere; and B is an unknown constant related to initial phase path caused by the unknown number of total phase rotations along the line of sight [*Afraimovich et al*., 2001; *Carrano and Groves*, 2009].

We have used the software "IONODETECT" developed at Council for Scientific and Industrial Research (CSIR) 4PI [*Vijayan et al*., 2013] which computes the relative IEC (IEC_R) by carrying out phase leveling along the phase-connected arc using both code and phase measurements independently. Phase leveling along the phase-connected arc is carried out to remove the noise in code and ambiguity in phase measurements.

$$IEC_R = IEC_\varphi + \left\langle IEC_p - IEC_\varphi \right\rangle_{arc} \tag{3}$$

IONODETECT applies the elevation mapping function (emf_θ) to the IEC_R to compute the vertical TEC in order to account for the discrepancy in the raypath length through the ionosphere as a function of GPS satellite elevation angle θ during the course of an orbital pass and the vertical TEC [*Calais and Minster*, 1995] or hereafter referred as TEC is given by

$$\begin{aligned} TEC &= \frac{IEC_R}{emf_\theta} \\ \text{where } emf_\theta &= \sec\left[\sin^{-1}\left(\frac{R}{R + h_{max}}\right)\cos(\theta)\right] \end{aligned} \tag{4}$$

R: radius of the Earth; h_{max}: height of maximum ionization.

For convenience sake, TEC is usually measured in TEC units TECU (1 TECU = 10^{16} el/m^2). TEC being an integral parameter makes it unfeasible to determine the height of TEC disturbance. However, the main contribution to TEC variations would occur around the height of the maximum ionization (h_{max}), which is in the ionosphere F_2 layer. Projection of the point of intersection of a line of sight with this thin F_2 layer on the Earth's surface is known as the subionospheric point (SIP). The propagation of CID is traced by this SIP. In this paper, the study region being the Indian equatorial and low-latitude sector, h_{max}, is assumed as 350 km [*Rama Rao et al*., 2006]. IONODETECT also calculates the CID in TEC following *Warnant and Pottiaux* [2000]

$$dTEC_R^S(t) = \frac{TEC_R^S(e_t) - TEC_R^S(e_{(t-1)})}{e_t - e_{(t-1)}} \tag{5}$$

where $dTEC_R^S(t)$ is the difference in TEC along raypaths of a satellite (S)-receiver (R) pair between two epochs e_t and $e_{(t-1)}$ and $TEC_R^S(e_t)$ is TEC along raypath of a satellite (S)-receiver (R) pair at epoch t.

To calculate the CID associated with an earthquake, the obtained dTEC is filtered using zero-phase bidirectional band-pass filter with passband of 1.67 to 16 mHz (1–10 min period). To investigate the characteristics of the ionospheric disturbances, CID propagation velocity and SIPs of lines of sight are also calculated.

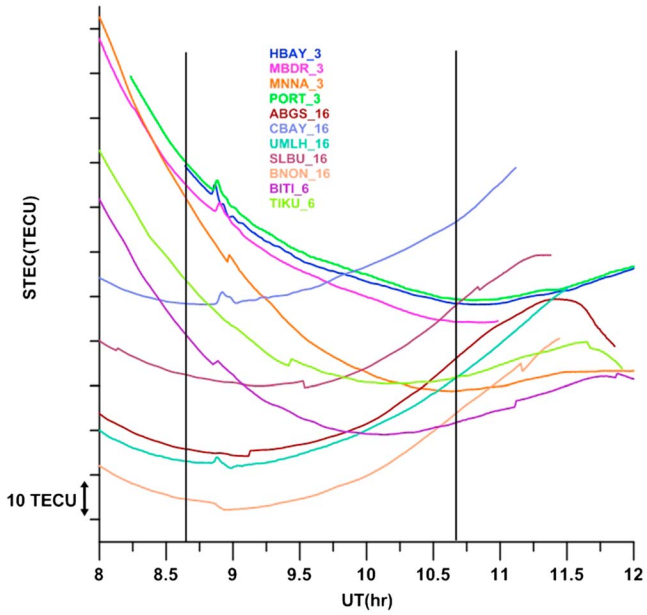

Figure 2. Time series of raw slant TEC changes observed at some of the stations used in the present study with satellites 3, 6, and 16. The black vertical lines indicate the occurrence of the M_w 8.6 main shock (8:38 UT) and M_w 8.2 aftershock (10:43 UT).

TEC measurements of satellites PRN 3, PRN 6, and PRN 16 are considered in the present study to understand the coseismic TEC perturbations in the Sumatra-Andaman region. In the present study, to understand the TEC disturbance due to the two events, we analyzed GPS data of 30 s sampling interval from the Sumatran GPS Array (SuGAr) (ftp://eos.ntu.edu.sg) as well as from the Andaman and Nicobar Islands and nearby International GNSS Service (IGS) stations (http://sopac.ucsd.edu/cgi-bin/dbDataByDate.cgi). In all the plots *d*TEC has been projected in TECU for 30 s sampling interval.

3. Observations and Results

3.1. TEC Anomalies of the 2012 Indian Ocean Earthquake

3.1.1. Coseismic Anomalies

The ionospheric response to the two great earthquakes is abstracted from GPS measurements recorded over a network of receivers distributed in the Sumatra and Andaman regions (see Figure 1) using satellites PRN 3, 6, and 16. The corresponding SIP trajectories at a representative GPS site LEWK are also shown. The raw slant TEC time series between 8 and 12 UT recorded by the satellites 3, 6, and 16 visible from few sites in Sumatra and Andaman-Nicobar Islands is shown in Figure 2. The TEC time series recorded by commonly visible satellites PRN 3 (Figure 1b) and PRN 16 (Figure 3b) during 8–12 UT over Sumatra and Andaman show that the CIDs are detected at most of the sites within 10–20 min and at some sites up to 30 min after the earthquake occurrence and up to distances of 1200 km from the epicenter. The amplitudes of the vertical TEC fluctuations or the CID signal (Figures 1b and 3b) vary between 0.02 and 0.7 TECU with a time period of 1–6 min. The high TEC fluctuations are observed at the Andaman GPS sites and at couple of northern Sumatra sites.

The CID propagation is not unidirectional but is bilateral (see Figures 1b and 3b), propagating from the epicenter to the Andaman in the north and Sumatra in the south. Taking advantage of the network of GPS stations in the study region, we now explore the temporal evolution of TEC. The temporal variations of the TEC can be comprehended from the travel diagram presented in Figure 4. The data presented correspond to each SIP for the common satellites PRN 3, PRN 6, and PRN 16 visible over the region. The slopes of the best fit lines suggest a velocity of 1262–930 m/s in the least squares sense. Thus, the velocity of the CID obtained in the present study corresponds to the acoustic wave (~1 km/s). Though the coseismic ionospheric disturbance is observed both north and south of the epicenter, the amplitude, velocity of CID, and their waveforms differ considerably. Within ~10–13 min after the quake, the northern Andaman GPS stations registered a typical *N*-type TEC disturbance with an amplitude of 0.9 TECU, whereas the southern Sumatra sites registered a TEC disturbance of 0.4 TECU. Observing a considerable difference in the TEC amplitudes and waveforms of Andaman and Sumatra regions, the propagation velocity of TEC disturbance is calculated independently for both regions. In the Andaman segment it is observed to be 2–3.5 km/s (Figure 5). Moreover, within Sumatra, the perturbation appears to be split into two separate waves, one observed till ~750 km of distance from the epicenter and the other beyond 750 km.

The separation of the TEC disturbance into two modes and their respective TEC amplitude variations are clearly noticeable in the traveltime diagram for PRN 3, 6, and 16 (Figure 4). It can be inferred from this figure that in the Sumatra region, south of the epicenter, up to a distance of ~750 km, the initial disturbance travels with an apparent velocity of about ~1 km/s, equals to the speed of the acoustic wave

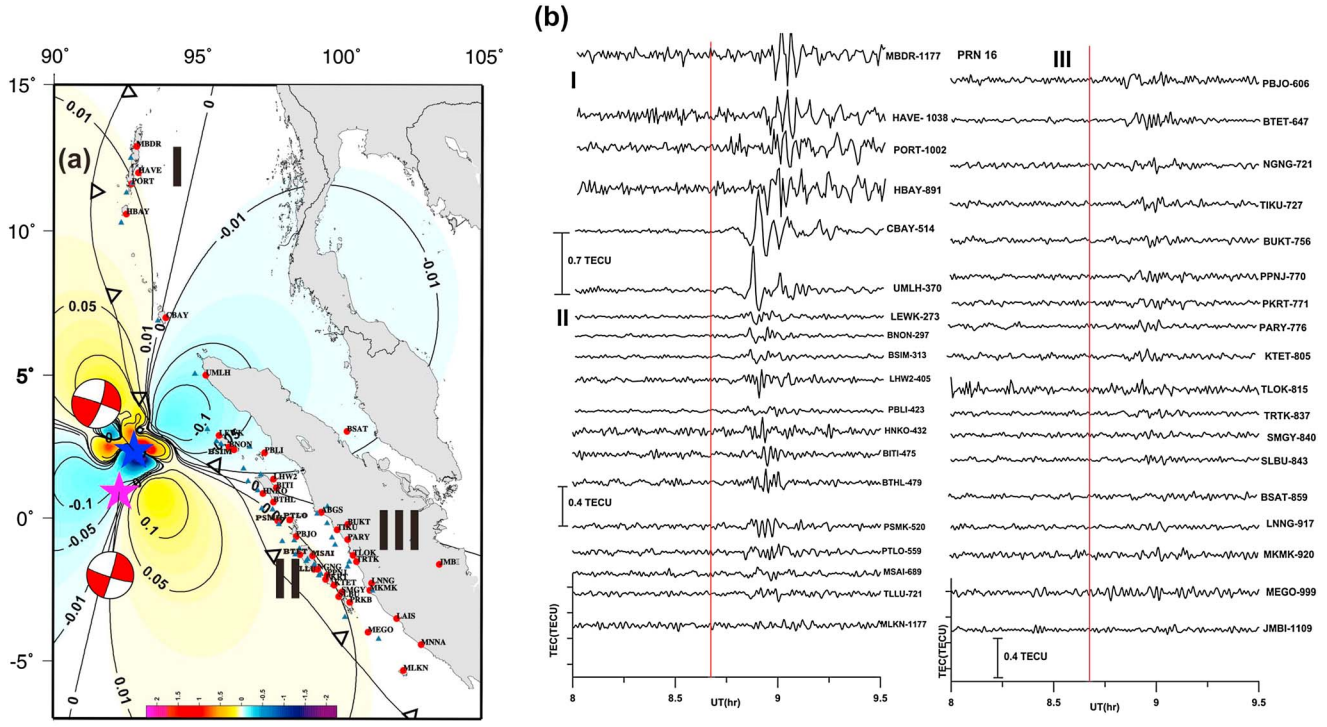

Figure 3. Contours of simulated coseismic vertical displacement (in meters) due to the 11 April 2012, M_w 8.6, Indian Ocean earthquake using the source model of *Yue et al*. [2012]. The blue and pink stars denote the epicenters of main shock and aftershock, respectively. Red solid circles are ground GPS receivers, and blue triangles are SIPs observed by satellite PRN 16. (b) Same as in Figure 1b but traces are coseismic TEC variation as observed by satellite PRN 16.

and between ~750 km and ~1400 km with a reduced speed of ~500–600 m/s (Figures 6b and 6c). However, in the Andaman region, north of the epicenter, the speed of perturbation is in the range of 2–3.5 km/s (Figure 6a). Hence, the component of TEC disturbance observed in the Andaman region with a velocity of 2–3.5 km/s may be termed "fast" and that observed in the group III of Sumatra segment with a velocity of ~600 m/s as "slow."

Comparable results were obtained from the records of satellite 16, albeit, with some variations in the amplitude arising out of the geometric differences in the lines of sight while observing the disturbance wavefront. The velocities observed by satellite 16 are 971 m/s for the waves in group II of Sumatra, 2 km/s for the fast component observed in the Andaman, and ~500 m/s for the slow component of the waves observed in group III of Sumatra (Figure 6). Ionospheric response to the aftershock (M_w 8.2) that occurred 2 h later at 10.43 UT on the same day is faint in the observations of PRN 3, PRN 6, and PRN 16 (Figure 4). But from the observations of PRN 32, similar pattern of separation of TEC disturbance is observed for this aftershock too. The TEC time series recorded by PRN 32 during 10.5–12 UT over Sumatra and Andaman is presented in Figure S1 in the supporting information. The propagation velocity of TEC disturbance in the Andaman region is 2.6 km/s, while in Sumatra region II, it is 1.3 km/s, and in region III, it is very insignificant (Figure S2).

Several other disturbances in the ionosphere such as geomagnetic storms, solar flares, and space weather can contribute to the observed TEC signals. It therefore becomes important to further substantiate our correlation of TEC with earthquake occurrence. We therefore compared our TEC measurements with *Dst* index variations, which are a measure of average change of the horizontal component of the geomagnetic field. These *Dst* index variations are a good proxy to most of the ionospheric disturbances and discriminate between a quiet and a disturbed day. The *Dst* index variations on the day of earthquake occurrence, a day prior to and later, are compared (Figure 7b). The corresponding *Dst* indices with reference values of −2 to 26 testify that the day of earthquake occurrence is a quiet day.

The *Dst* indices indeed tabulate 11 April 2012 as an International Quiet Day (http://www.ga.gov.au/oracle/geomag/display_iqd.jsp). It is obvious from Figure 7a that the TEC variations at several stations are at the

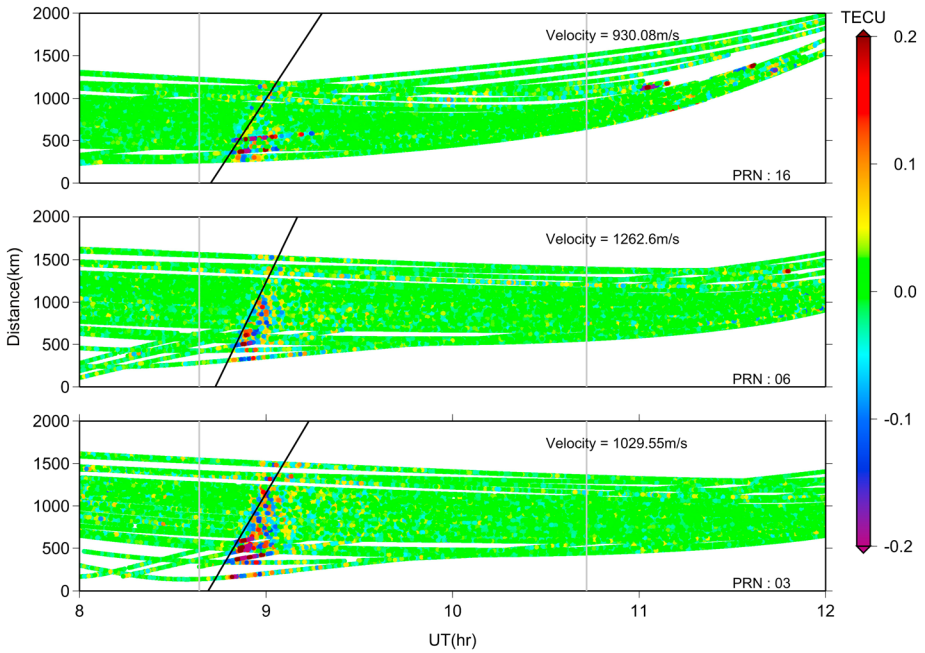

Figure 4. Traveltime diagram of band pass-filtered TEC in response to the 11 April 2012 earthquake at the SIPs to the epicenter as recorded by satellites PRN 3, PRN 6, and PRN 16. Vertical thick lines indicate the time of the main shock and the aftershock at 8:38 UT and 10:43 UT, respectively. The slanted black line shows the best fit of the CID arrival times denoting the propagation velocities of ionospheric TEC disturbance. The distances are great circle distances between SIPs and the epicenter.

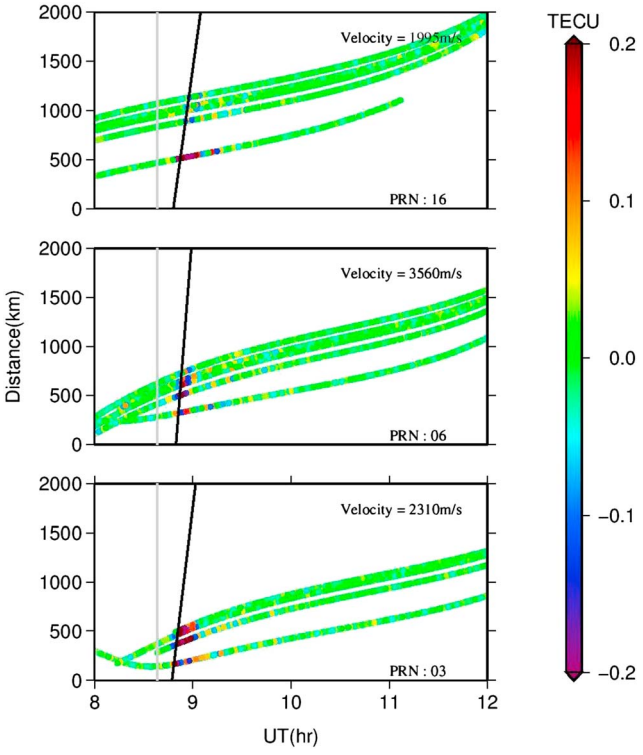

Figure 5. Same as in Figure 4 but the travel diagram of band pass-filtered TEC is for the sites in Andaman, north of the epicenter.

background level on the reference days, while on the day of earthquake occurrence the observed TEC anomaly stands out. The observed anomalous TEC signals at ~8.8 UT on this quiet geomagnetic day can therefore be attributed to the earthquake occurrence (8.6 UT) with a fair degree of confidence.

3.1.2. Far-Field Observations

In view of the predominant strike-slip mechanism of the 11 April 2012 great earthquake, it would be interesting to document the behavior of distant sites (>2000 km from the epicenter) and record the related ionospheric response if any. For this purpose, well-established GPS stations BAKO, IISC, HYDE, XMIS, PALK, COCO, NTUS, and DGAR covering a wide distance range are analyzed (Figure 8). Clear CID arrivals in the time window 15–22 min with a time period of about 2–5 min are recorded by most of these far-field locations. The TEC amplitudes vary between 0.04 and 0.2 TECU. The magnitude of the aftershock being lower than the main shock, the TEC time series is less complex (see Figure S1). Following the

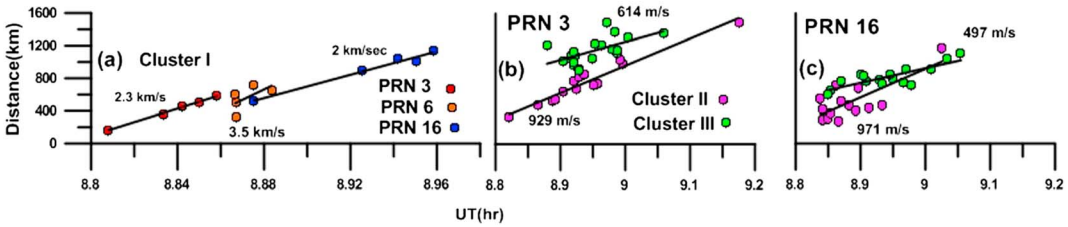

Figure 6. Time-distance plot to represent propagation velocities in the clusters I, II, and III indicated in Figure 3a. The distances are great circle distances between SIPs and the epicenter. (a) For the sites in Andaman with satellites 3, 6, and 16. (b) For the sites of Sumatra in clusters II and III with satellite 3. (c) With satellite 16.

aftershock of M_w 8.2, HYDE and PIMO seem to illustrate quasiperiodical TEC oscillations [*Astafyeva and Afraimovich*, 2006] with a time period of about 2–6 min. After the occurrence of the aftershock, the disturbance arrived at HYDE station, situated at an epicentral distance of ~2000 km, within 13 min and continued for ~60 min, while the disturbance that arrived at PIMO, which is 3500 km from the epicenter, after 1.5 h continued for ~75 min (Figure 8b). The rest of the IGS sites do not show any appreciable change in TEC for the aftershock. The directivity of the ionospheric disturbances observed in the far field is on expected lines of the surface wave radiation pattern of the earthquake [*Duputel et al*., 2012] and hence is supposed to be excited by the potent surface Rayleigh waves of the 11 April 2012 Indian Ocean earthquake.

4. Discussion

4.1. Inconsistencies in Observed CID Waveforms/Amplitudes—Possible Sources

The amplitude of the TEC disturbance from the epicenter decreases gradually in the groups II and III of Sumatra region. The same observation can be seen even in the Andaman region (I). However, the amplitudes in region I, north of the epicenter, are greater compared to those in Sumatra region (south of the epicenter) for the same distance from the epicenter (Figures 1b and 3b).

Though polarities of ionospheric disturbance waveforms (Figure 3b) are mostly consistent with the coseismic vertical ground motion due to the 2012 Indian Ocean earthquake, some discrepancies can be noticed. Recognizing that several factors ranging from complex rupture of the earthquake, use of sampling interval of 30 s, and effects of geometry of line of sight [*Afraimovich et al*., 2001; *Astafyeva and Heki*, 2009; *Heki and Ping*, 2005] could influence the CID amplitudes and waveforms, in the following, we discuss the possible sources for the observed inconsistencies.

For example, the discrepancy in the CID amplitudes at site UMLH observed by satellites 3 (Figure 1b) and 16 (Figure 3b) arises from attendant differences in the incidence angles (shallow or deep) between the corresponding line of sight and the wavefront [*Cahyadi and Heki*, 2013]. This also results in coherence of the phases of the point sources leading to recording of high CID peaks as seen at UMLH by PRN 16. Further, the difference in the apparent CID amplitudes at the same site for different satellites can also stem from the three-dimensional structure of the CID in the ionosphere of finite thickness [*Heki and Ping*, 2005]. The delineated SIPs in this study are not close to the earthquake rupture zones, and hence, the observed CID amplitudes in our study may not reflect the complexities of the rupture process but instead record the effect of rupture in terms of displacements. It can be seen from Figure 3a that the CID origins located SE of the epicenter at distances about 500–1300 km coincide with the contour of vertical coseismic crustal displacements of <1 cm [*Yue et al*., 2012]. At such a distance from the epicenter, the acoustic origin CID might have decayed considerably [*Heki and Ping*, 2005]. This reiterates that the incidence angle of the line of sight is one of the factors that contribute significantly to the measured CID amplitudes [*Heki et al*., 2006] in the present study.

As discussed above, the polarities of the ionospheric disturbance waveforms (Figure 3b) are consistent with the coseismic vertical ground motion due to the 2012 Indian Ocean earthquake. The inconsistencies in some of the waveforms can arise when the ionospheric disturbance does not exactly follow the source waves coming from below but instead travels along the phase of the superimposing source wave [*Astafyeva and*

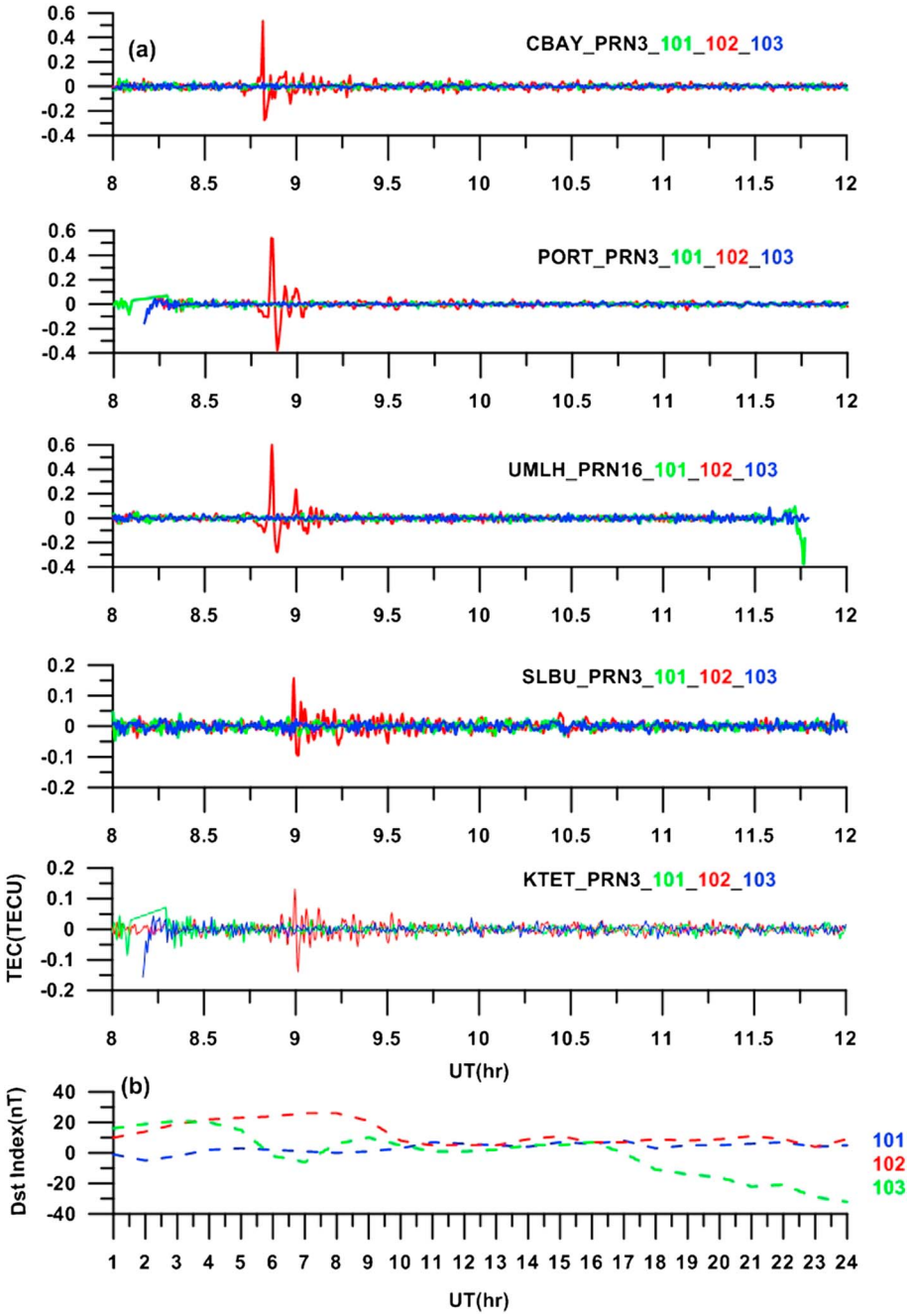

Figure 7. (a) Temporal variation of band pass-filtered TEC at some of the sites of Andaman-Sumatra Islands on the day of the earthquake (102), the day before earthquake (101), and the day after the earthquake (103). (b) Variation of *Dst* indices on Julian days 101, 102, and 103.

Heki, 2009]. Deviations observed from these wave shapes at some sites can also arise due to inadequate sampling interval (30 s) and/or poor line-of-sight geometry besides the 3-D structure of the CID. The coseismic vertical displacements for the M_w 8.6 earthquake presented in Figure 3a are based on the model characteristics of *Yue et al.* [2012]. The observed TEC response has an *N* wave shape over the regions of uplift in Andaman. The number of available sites in the subsidence region is small, and a perceptible inverted *N* wave is not visible. Moreover, since the vertical displacements experienced at the rest of the sites of the present study are quite small, the kind of CID polarities for uplift and subsidence as observed for a dip-slip earthquake are not clearly noticeable for this strike-slip earthquake.

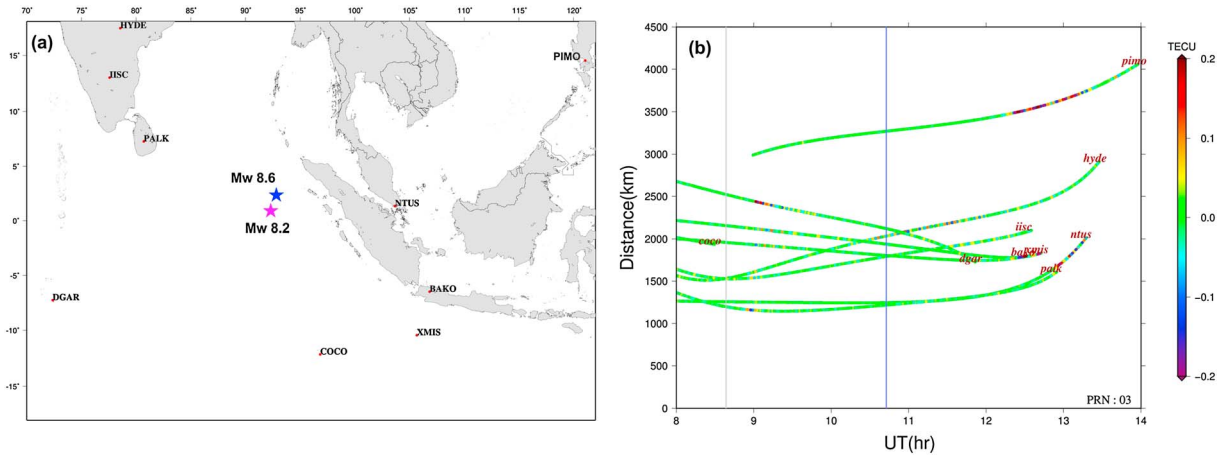

Figure 8. (a) Locations of far-field GPS stations used in the present study. Blue and pink stars denote the epicenters of the main shock and the aftershock, respectively. Stations are denoted by four-letter codes. (b) Hodochrone of band pass-filtered TEC at some of the far-field IGS sites. The solid vertical lines denote the time of the main shock of M_w 8.6 at 8:38 UT and aftershock of M_w 8.2 at 10:43 UT.

4.2. CID Propagation Speeds

In the present study, at majority of the GPS sites located in Sumatra and Andaman, at distances up to 1200 km, the CIDs are detected within 10–20 min after the occurrence of the main shock. Their average propagating velocity of 1262–930 m/s (Figure 4) suggests that these CIDs are indeed induced by shock acoustic waves [*Afraimovich et al*., 2001] of the 11 April 2012 Indian Ocean earthquake. The small deviation of the propagating velocity from shock acoustic waves (1 km/s) could be due to the effects of geometry of line of sight and errors of the measurement. The CIDs are better pronounced in the Andaman region, north of the epicenter, compared to the Sumatra region to the south (Figures 1b and 3b). In addition, here we notice the trend of CID separating into two modes. Near the epicenter in Sumatra region (marked as II in Figure 3a) up to a distance of 750 km, the CID travels with a velocity of ~ 1 km/s (Figure 6). This velocity represents the speed of sound at the height of ionosphere *F* layer. Starting from ~600 to 750 km from the epicenter, the disturbance appears to be divided into two perturbations which travel with different velocities: one wave propagating with a speed of 2–3.5 km/s toward Andaman in the north and the other with a velocity of 500–600 m/s to the cluster III of Sumatra region. This region is far southeast of the epicenter and the SIPs of cluster III sites are lying in the neutral region. Thus, within a distance of ~1400 km from the epicenter there appears splitting of TEC disturbance and its propagation with differing velocities in different directions. The shape and amplitude of the CID in Andaman is very lucid and consistent from 500 to 1200 km consistent with the propagating Raleigh wave [*Kakinami et al*., 2013], while it seems to be a mixture of signals in the Sumatra region (Figures 1b and 3b). Hence, it can be comprehended that the fast mode propagating with a velocity of 2–3.5 km/s may be attributed to surface Rayleigh waves. On the other hand, the mode of TEC disturbance traveling with a velocity of ~1 km/s in the cluster II of Sumatra region is of acoustic origin, while that in cluster III with a velocity of ~500–600 m/s may be termed as slow component of the split TEC disturbance as the acoustic gravity waves do not appear to be induced by the shock waves of the present earthquake. Moreover, the tsunamigenic waves are not reported for the 11 April 2012 Indian Ocean earthquake as the vertical displacement due to the earthquake was only on the order of 1.5 m [*Occhipinti et al*., 2013].

Propagation velocities, waveforms, and periods of ionospheric perturbations depend on their origin as well as the distance from the epicenter. The propagation velocity of ionospheric disturbances in the cluster III region is estimated to be 500–600 m/s. These disturbances might be induced by the acoustic waves generated due to the vertical ground motion of the quake itself [*Astafyeva et al*., 2009], which reach the ionosphere at a different angle, and by this virtue, the CID travels horizontally. This region is far southeast of the epicenter, and SIPs of cluster III are lying in the neutral region (Figure 3a). Velocities of 600 m/s can be attributed to acoustic waves in the far field [*Astafyeva et al*., 2009]. Moreover, there is a time lag of ~ 5 min between the first arrival of CID in regions II and III. It appears from Figure 1b that the TEC response in the Sumatra region is a mixture of signals which are observed as two separate modes owing to the

difference in their velocities. The possible reasons for the observed slow component of velocity could arise due to multiple sources like distance from the epicenter as well as to the line-of-sight geometry and the azimuthal difference in energy emission of seismic waves [*Calais et al*., 1998].

The range of magnetic inclination angle (12° to −26°) in the study region is parallel to the magnetic field lines. The ionospheric coupling factor is less to influence the source directivity (Figure S3). Hence, among these factors, the anomalous azimuthal variation in Rayleigh wave amplitude attributed to source directivity (effects) could have resulted in preferential northward propagation of disturbances compared to those observed toward south and southeast directions of the epicenter. Therefore, source directivity-related effects emerge as the potential driving mechanism to explain our observation. This kind of separation of TEC disturbance has been reported by *Astafyeva et al*. [2009] for the great Kurile earthquake of 4 October 1994 in which the perturbation propagated only in one direction, i.e., southward.

4.3. Intraplate Versus Subduction Zone Earthquakes

The response of the ionosphere to the ground displacements caused by an earthquake is varied and diverse depending on the focal mechanism of earthquake, its magnitude, and the physical conditions prevailing in the atmosphere at the time of earthquake occurrence. Many interesting results have been published from the study of different earthquakes and specifically the recent *M* 9.0 Tohoku earthquake due to the available data from dense GPS networks. We would like to discuss the results of the present study in the light of Tohoku earthquake results.

At the outset these two earthquakes cannot be compared directly as the mechanisms, magnitudes, and tectonic environments in which 2012 Indian Ocean earthquake and 2011 Tohoku earthquake occurred are quite different. The tsunamigenic *M* 9.0 Tohoku earthquake occurred as a result of thrust faulting near the subduction zone interface plate boundary between the Pacific and North American Plates with a bilateral rupture dimension of 300 × 150 km and with a reported uplift of 5–8 m. In contrast, the *M* 8.6 Indian Ocean earthquake is the largest intraplate strike-slip earthquake devoid of tsunami, with a slip as large as 30 m, depth extent of the rupture 40 km into the upper mantle, and an uplift of ~1.5 m. Both the earthquakes are powerful and occurred near the dense GPS networks and yielded signatures of Rayleigh waves, acoustic waves, and slow component of acoustic waves. However, as the Indian Ocean earthquake did not generate a tsunami, the acoustic gravity waves are not noticeable. The north-south asymmetry of the CID excited by the Rayleigh wave is observed for both the earthquakes. Further, *Kakinami et al*. [2013] concluded that a CID associated with the Rayleigh wave is detected when the angle of oscillation of the superimposed wavefront is close to being parallel to the magnetic field lines. Though in the case of Indian Ocean earthquake the magnetic inclination (12 to −26°) throughout the study region (i.e., in Andaman and Sumatra) is parallel to the magnetic field lines and the ionospheric coupling factor being a little more in Sumatra compared to that in Andaman (Figure S3), yet the CID induced by the Rayleigh wave is not apparent in the Sumatra region suggesting the limited role of magnetic inclination in our observations. Hence, the observations of Indian Ocean earthquake indicate that the north-south asymmetry of the CID excited by the Rayleigh wave can be attributed to their anomalous azimuthal variation in the radiation pattern. In both these earthquakes, the waves pertaining to slow component of acoustic waves propagated for more than 1000 km from the epicenter. In the case of Tohoku earthquake they were attributed to gravity modes of the coseismic atmospheric waves [*Tsugawa et al*., 2011], while for the Indian Ocean earthquake the driving mechanism seems to be different (as described in section 4.2) due to absence of acoustic gravity waves.

4.4. Directivity of CID Propagation

The distribution of the GPS sites used in the present study covers a wide azimuth range, unlike in the past, and thus enables us to map directivity patterns in CID propagation with reduced ambiguity. Conflicting results obtained for some recent past earthquakes that occurred in this study region, largely due to paucity of observations over a wide azimuth range then, made this issue contentious. In an earlier study, *Heki and Ping* [2005] proposed that in the Northern Hemisphere, the ambient magnetic field attenuates northward propagation of CID. This favored southward propagating disturbances and attenuation of northward propagating disturbances. A reversed observation was reported for the Southern Hemisphere 2007 Bengkulu earthquake [*Cahyadi and Heki*, 2013] in support of the above proposed model. However, as

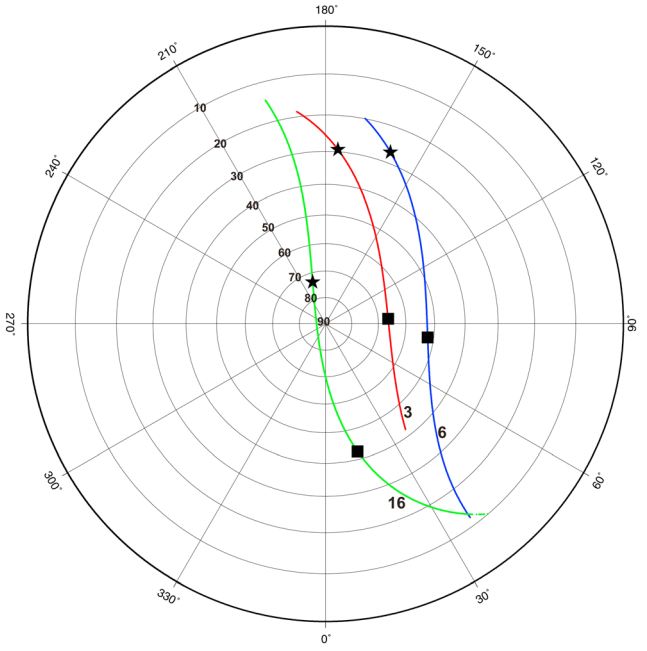

Figure 9. Polar plot of the elevation and azimuth angles of satellites 3, 6, and 16 as observed by a site in Andaman during 8–13 UT. The star and the square mark the position of the satellites at the time of the main shock (8:38 UT) and aftershock (10:43 UT), respectively.

most of the sites related to the Bengkulu earthquake observations are predominantly located north of the fault, the reported preferential northward CID propagation remains largely unsubstantiated due to lack of stations toward the south. For the 2004 Sumatra-Andaman earthquake too, significant TEC disturbances to the north of the epicenter are recorded compared to smaller TEC variations southward [*Otsuka et al*., 2006]. It is therefore important to recall that the rupture of both these earthquakes propagated only in the northward direction. Nevertheless, it is pertinent to note that the 2004 Sumatra-Andaman earthquake and 2007 Bengkulu earthquake occurred in the equatorial region rather than in the Southern Hemisphere to fully validate the model of *Heki and Ping* [2005] for CID directivity.

In the case of the 2012 earthquake, the ionospheric radiation pattern appears to have followed the complex rupture geometry, thereby propagating in all the directions. Although it is observed in the north, south, and east directions around the epicenter, it could not be mapped in the westerly direction due to the absence of sites in that particular direction. The observed TEC enhancement in northern and southern directions (Figure 1b) seems consistent with the model predictions of *Heki and Ping* [2005] that accommodates both northward and southward propagation of TEC in the equatorial regions. The low-amplitude TEC disturbances observed by the line of satellites 3 and 16 in the cluster III of Sumatra compared to cluster II of Sumatra (Figures 1b and 3b) may be attributed to their distance from the epicenter as well as to the line-of-sight geometry and the azimuthal difference in energy emission of seismic waves [*Calais et al*., 1998]. Though the rupture-generated vertical displacements are quite low (Figure 3a), ionospheric waves are reported. High TEC amplitude is observed only at the northern sites of Andaman although some of the southern sites of the Sumatra region are at the same distance from the epicenter.

According to *Rolland et al*. [2011], the optimum condition of satellite elevation angle being less than 40° for efficient detection of Rayleigh wave-induced ionospheric disturbances is satisfied by satellites 3 and 6 (Figure 9). Although the elevation angle of satellite 16 is almost vertical, the propagation speed of TEC perturbation detected in Andaman is 2 km/s (Figure 5). This is much higher than the acoustic wave speed but very much close to Rayleigh wave speeds. Hence, the TEC perturbation speed observed in Andaman though dependent on elevation angle of the satellite, yet the causative source, is more likely due to Rayleigh waves.

We illustrate the ionospheric coupling factor (α) defined as the cosine of the angle between the neutral velocity and geomagnetic field vectors [*Calais et al*., 1998] in Figure S3 using a radial wave vector "*k*"with a zenith angle of 10° [*Rolland et al*., 2011]. The ionospheric coupling factor map for the 2012 Indian Ocean earthquake shows that ionospheric coupling is less in the north ($\alpha = 0.1–0.3$) than in the south ($\alpha = 0.2–0.6$). It can be observed that in overall the coupling factor is less in the region of the present study. In spite of the coupling factor being less in the Andaman compared to south of the epicenter, the amplitude of signal and the speed of ionospheric perturbation are more in cluster I (Andaman) compared to that in Sumatra (cluster II and cluster III). But it has been demonstrated by *Rolland et al*. [2011] that the ionospheric coupled wave is less attenuated toward the region where the ionospheric coupling factor is more. Our observations are contrary to the model explained. Hence, the observed anisotropy is more

related to Rayleigh wave radiation pattern than to the geomagnetic field effect. Furthermore, for 2012 Indian Ocean earthquake, *Duputel et al*. [2012] reported anomalous azimuthal variation of Rayleigh wave amplitude ascribed to the source effects. It has been shown for the 2011 Tohoku earthquake that the CID related to the Rayleigh wave was observed only south of the epicenter, and this asymmetry was accredited to the ambient magnetic field inclination [*Kakinami et al*., 2013]. But the CID related to the Rayleigh wave in the case of 2012 Indian Ocean earthquake was observed only north of the epicenter, in spite of low ionospheric coupling factor. Therefore, among the three elements viz., the seismic source, geomagnetic field, and the observation geometry which govern the north-south anisotropy and the propagation of Rayleigh wave-induced perturbation, the focal mechanism and rupture of the earthquake have obviously played the key role.

4.5. Influence of Equatorial Ionization Anomaly on CID

EIA (equatorial ionization anomaly) is a spatial variability in ionization density and TEC due to the "fountain effect" set up by the interaction of the diurnal variation of the zonal electric field with the horizontal geomagnetic field at the equatorial region causing uplift of the plasma by $E \times B$ drift [*Anderson*, 1981; *Walker et al*., 1994]. Since the earthquake of the present study occurred in the equatorial region at the local time 14:38 h, a well-formed EIA must be present during the main shock as well as aftershock that occurred 2 h later. In order to assess the influence of EIA-induced spatial variability of TEC on the amplitude variation and N-S directivity of the CID, we have computed the percentage of relative TEC perturbation over the background TEC at each SIP during the time of observation.

$$\text{Relative } d\text{TEC} = (d\text{TEC}/\text{TEC})*100 \tag{6}$$

We have examined this for the sites of clusters I, II, and III. Comparison between *d*TEC and relative *d*TEC (Figure S4) clearly depicts that the amplitude difference in the northward and southward propagating CIDs is independent of the background TEC. This suggests that the CIDs of the present study might not have been influenced by the EIA but rather an apparent manifestation of seismic origin.

5. TEC Anomalies of the Aftershock

The main earthquake M_w 8.6 was followed by an aftershock of magnitude (M_w) 8.2, on the same day, 2 h later, at a distance of 180 km SSW of the main shock with a similar focal mechanism. Though satellites 3, 6, and 16 are visible over the region at the time of this aftershock occurrence, in general, appreciable TEC variation is not observed. The travel diagram from the observations of satellites 3 and 6 (Figure 4) shows no discernible TEC variation at all the sites except HAVE in the Andamans. However, satellites 16 and 32 (Figures 4 and S1) documented CIDs of aftershock. This again demonstrates the sensitivity to the elevation angle of the satellite. At the time of aftershock, the SIPs of satellites 3 and 6 have high elevation angles of around 65° and 55° while that of satellite 16 is around 40°. Moreover, the finite-fault slip model for this aftershock by *Yue et al*. [2012] shows a maximum displacement of ~58 cm at the source (Figure S1), which is about half that observed for the main shock, and correspondingly, the amplitude of aftershock TEC disturbance is less than that of the main shock. SIPs of the aftershock are close to the neutral contour and contours of vertical displacement < 5 mm. In this case too, the observed CIDs arrived 12–18 min after the incidence of aftershock and the TEC disturbance is split into differing velocities of propagation. Seismic moment of the aftershock is approximately one fourth of the main shock.

6. Conclusions

In the present study we have demonstrated that the coseismic ionospheric perturbation related to the 11 April 2012 Indian Ocean earthquake is influenced by uncharacteristic discrepancy of Rayleigh wave amplitudes generated by this M_w 8.6 strike-slip mechanism earthquake. Both near-field and far-field sites responded to this earthquake. The characteristics such as propagation speed and the directivity of the CIDs of this unique earthquake are studied. The ionospheric disturbances arrived at most of the GPS sites within 10–18 min after the earthquake. The TEC waveforms by and large are consistent with the focal mechanism of the earthquake. The direction of CID propagation is not unidirectional but has propagated effectively both to the north and south of the epicenter with different propagation velocities and thereby indicating the separation of TEC disturbance into two different modes. The ionospheric disturbance direction pattern appears to have followed the rupture geometry.

The observed CID propagation can be attributed to the Rayleigh wave radiation pattern than the effects of geomagnetic field as already discussed. The relatively low vertical displacement of 1 m compared to similar magnitude dip-slip earthquakes at the epicenter and less than 1 m at the GPS sites used in the present study could effectively amplify the ionospheric perturbation throughout the study region, as evident from their excellent spatial and temporal correlation.

Tabulation of the day of earthquake occurrence as an International Quiet Day together with the detected low *Dst* and background TEC values on the days prior to and after the earthquake suggests that the observed TEC fluctuation is a direct consequence of earthquake occurrence. EIA does not appear to have influenced the amplitude and directionality of the CIDs observed in the present study.

Acknowledgments

We acknowledge the scientific and technical staff of EOS and LIPI for making SuGAr data available to carry out this work. The continuous GPS data from Andaman-Nicobar can be downloaded on request from the website (www.isgn.gov.in). Amit Bansal, M. Narsaiah, Simhadri Naidu, and Rajeshwar Rao helped in the Andaman-Nicobar region field work and data management. The GPS work in the Andaman and Nicobar region is financially supported by the Ministry of Earth Sciences. Rajeev Yadav and Bhaskar helped with some of the figures presented in the work. Discussion with Lucie Rolland has clarified some of our doubts and helped in improving the manuscript. We thank Masashi Kamogawa and an anonymous reviewer for their constructive reviews. CSIR-NGRI PROJECT ARiEES (Advance Research in Engineering and Earth Sciences) is a part of DREAMS Research for Earthquake Hazard Assessment by Modelling the Solid-Earth project. We thank Gloria Varghese for her help in computing TEC.

Michael Liemohn thanks the reviewers for their assistance in evaluating this paper.

References

Afraimovich, E. L., N. P. Perevalova, A. V. Plotnikov, and A. M. Uralov (2001), The shock-acoustic waves generated by the earthquakes, *Ann. Geophys.*, *19*, 395–409.

Anderson, D. N. (1981), Modeling the ambient, low latitude F-region ionosphere—A review, *J. Atmos. Sol. Terr. Phys.*, *43*, 753–762.

Artru, J., T. Farges, and P. Lognonné (2004), Acoustic waves generated from seismic surface waves: Propagation properties determined from Doppler sounding observations and normal-mode modeling, *Geophys. J. Int.*, *158*, 1067–1077.

Astafyeva, E. I., and E. L. Afraimovich (2006), Long-distance propagation of travelling ionospheric disturbances caused by the great Sumatra-Andaman earthquake on 26 December 2004, *Earth Planets Space*, *58*, 1025–1031.

Astafyeva, E., and K. Heki (2009), Dependence of waveform of near-field coseismic ionospheric disturbances on focal mechanisms, *Earth Planets Space*, *61*, 939–943.

Astafyeva, E., K. Heki, V. Kiryushkin, E. Afraimovich, and S. Shalimov (2009), Two-mode long-distance propagation of coseismic ionospheric disturbances, *J. Geophys. Res.*, *114*, A10307, doi:10.1029/2008JA013853.

Astafyeva, E., L. M. Rolland, and A. Sladen (2014), Strike-slip earthquakes can also be detected in the ionosphere, *Earth Planet. Sci. Lett.*, *405*, 180–193, doi:10.1016/j.epsl.2014.08.024.

Cahyadi, M. N., and K. Heki (2013), Ionospheric disturbances of the 2007 Bengkulu and the 2005 Nias earthquakes, Sumatra, observed with a regional GPS network, *J. Geophys. Res. Space Physics*, *118*, 1777–1787, doi:10.1002/jgra.50208.

Calais, E., and J. B. Minster (1995), GPS detection of ionospheric perturbations following the January 17, 1994, Northridge earthquake, *Geophys. Res. Lett.*, *22*, 1045–1048, doi:10.1029/95GL00168.

Calais, E., and J. B. Minster (1998), GPS, earthquakes, the ionosphere, and the Space Shuttle, *Phys. Earth Planet. Inter.*, *105*, 167–181.

Calais, E., J. B. Minister, M. A. Hofton, and M. A. H. Hedlin (1998), Ionospheric signature of surface mine blasts from Global Positioning System measurements, *Geophys. J. Int.*, *132*, 191–202.

Carrano, C., and K. Groves (2009), *Ionospheric Data Processing and Analysis, Workshop on Satellite Navigation Science and Technology for Africa*, The Abdus Salam ICTP, Trieste, Italy.

Davies, K. (1990), *Ionospheric Radio*, Peter Peregrinus, London.

Ducic, V., J. Artru, and P. Lognonné (2003), Ionospheric remote sensing of the Denali earthquake Rayleigh surface waves, *Geophys. Res. Lett.*, *30*(18), 1951, doi:10.1029/2003GL017812.

Duputel, Z., H. Kanamori, V. C. Tsai, L. Rivera, L. Meng, J.-P. Ampuero, and J. M. Stock (2012), The 2012 Sumatra great earthquake sequence, *Earth Planet. Sci. Lett.*, *351–352*, 247–257, doi:10.1016/j.epsl.2012.07.017.

Heki, K., and J. Ping (2005), Directivity and apparent velocity of the coseismic ionospheric disturbances observed with a dense GPS array, *Earth Planet. Sci. Lett.*, *236*, 845–855.

Heki, K., Y. Otsuka, N. Choosakul, N. Hemmakorn, T. Komolmis, and T. Maruyama (2006), Detection of ruptures of Andaman fault segments in the 2004 great Sumatra earthquake with coseismic ionospheric disturbances, *J. Geophys. Res.*, *111*, B09313, doi:10.1029/2005JB004202.

Kakinami, Y., M. Kamogawa, S. Watanabe, M. Odaka, T. Mogi, J. Y. Liu, Y. Y. Sun, and T. Yamada (2013), ionospheric ripples excited by superimposed wavefronts associated with Rayleigh waves in the thermosphere, *J. Geophys. Res. Space Physics*, *118*, 905–911, doi:10.1002/jgra.50099.

Liu, J. Y., Y. B. Tsai, S. W. Chen, C. P. Lee, Y. C. Chen, H. Y. Yen, W. Y. Chang, and C. Liu (2006), Giant ionospheric disturbances excited by the M9.3 Sumatra earthquake of 26 December 2004, *Geophys. Res. Lett.*, *33*, L02103, doi:10.1029/2005GL023963.

Liu, J. Y., H. F. Tsai, C. H. Lin, M. Kamogawa, Y. I. Chen, C. H. Lin, B. S. Huang, S. B. Yu, and Y. H. Yeh (2010), Coseismic ionospheric disturbances triggered by the Chi-Chi earthquake, *J. Geophys. Res.*, *115*, A08303, doi:10.1029/2009JA014943.

Liu, J. Y., C. H. Chen, C. H. Lin, H. F. Tsai, C. H. Chen, and M. Kamogawa (2011), Ionospheric disturbances triggered by the 11 March 2011 M9.0 Tohoku earthquake, *J. Geophys. Res.*, *116*, A06319, doi:10.1029/2011JA016761.

Lognonné, P., E. Clévédé, and H. Kanamori (1998), Computation of seismograms and atmospheric oscillations by normal mode summation for a spherical Earth model with realistic atmosphere, *Geophys. J. Int.*, *135*, 388–406, doi:10.1046/j.1365-246X.1998.00665.x.

Meng, L., J.-P. Ampuero, Z. Duputel, Y. Luo, and V. C. Tsai (2012), Earthquake in a maze: Compressional rupture branching during the 2012 Mw 8.6 Sumatra earthquake, *Science*, *337*, 724–726.

Occhipinti, G., L. Rolland, P. Lognonne, and S. Watada (2013), From Sumatra 2004 to Tohoku-Oki 2011: The systematic GPS detection of the ionospheric signature induced by tsunamigenic earthquakes, *J. Geophys. Res. Space Physics*, *118*, 3626–3636, doi:10.1002/jgra.50322.

Otsuka, Y., et al. (2006), GPS detection of total electron content variations over Indonesia and Thailand following the 26 December 2004 earthquake, *Earth Planets Space*, *58*, 159–165.

Pollitz, F. F., R. S. Stein, V. Sevilgen, and R. Burgmann (2012), The 11 April 2012 east Indian Ocean earthquake triggered large aftershocks worldwide, *Nature*, *490*, 250–253, doi:10.1038/nature11504.

Rama Rao, P. V. S., K. Niranjan, D. S. V. V. D. Prasad, S. Gopi Krishna, and G. Uma (2006), On the validity of the ionospheric pierce point (IPP) altitude of 350 km in the Indian equatorial and low-latitude sector, *Ann. Geophys.*, *24*, 2159–2168.

Rolland, L. M., P. Lognonné, and H. Munekane (2011), Detection and modeling of Rayleigh wave induced patterns in the ionosphere, *J. Geophys. Res.*, *116*, A05320, doi:10.1029/2010JA016060.

Rolland, L. M., M. Vergnolle, J.–M. Nocqet, A. Sladen, J.-X. Dessa, F. Tavakoli, H. R. Nankali, and F. Cappa (2013), Discriminating the tectonic and non-tectonic contributions in the ionospheric signature of the 2011, M_w7.1, dip-slip Van earthquake, Eastern Turkey, *Geophys. Res. Lett.*, *40*, 2518–2522, doi:10.1002/grl.50544.

Tsugawa, T., A. Saito, Y. Otsuka, M. Nishioka, T. Maruyama, H. Kato, T. Nagatsuma, and K. T. Murata (2011), Ionospheric disturbances detected by GPS total electron content observation after the 2011 off the Pacific coast of Tohoku Earthquake, *Earth Planets Space*, *63*, 875–879, doi:10.5047/eps.2011.06.035.

Vijayan, M. S. M., G. Varghese, and K. Shimna (2013), IONODETECT: A software to compute Ionospheric TEC perturbations using dual frequency geodetic GPS data, Annual Report 2012–2013, CSIR 4PI, pp. 77–79.

Walker, G. O., J. H. K. Ma, and E. Golton (1994), The equatorial ionospheric anomaly in electron content from solar minimum to solar maximum for South East Asia, *Ann. Geophys.*, *12*, 195–209.

Warnant, R., and E. Pottiaux (2000), The increase of the ionospheric activity as measured by GPS, *Earth Planets Space*, *52*(11), 1055–1060.

Yadav, R. K., B. Kundu, K. Gahalaut, J. Catherine, V. K. Gahalaut, A. Ambikapathy, and M. S. Naidu (2013), Coseismic offsets due to the 11 April 2012 Indian Ocean earthquakes (M_w 8.6 and 8.2) derived from GPS measurements, *Geophys. Res. Lett.*, *40*, 3389–3393, doi:10.1002/grl.50601.

Yue, H., T. Lay, and K. D. Koper (2012), En echelon and orthogonal fault ruptures of the 11 April 2012 great intraplate earthquake, *Nature*, *490*, 245–249, doi:10.1038/nature11492.

Yuen, P. C., P. F. Weaver, R. K. Suzuki, and A. S. Furumoto (1969), Continuous traveling coupling between seismic waves and the ionosphere evident in May 1968 Japan earthquake data, *J. Geophys. Res.*, *74*(9), 2256–2264, doi:10.1029/JA074i009p02256.